Science Advances
AAAS

advances.sciencemag.org/cgi/content/full/5/8/eaaw9298/DC1

Supplementary Materials for

Cushing's syndrome driver mutation disrupts protein kinase A allosteric network, altering both regulation and substrate specificity

Caitlin Walker, Yingjie Wang, Cristina Olivieri, Adak Karamafrooz, Jordan Casby, Kerstin Bathon, Davide Calebiro, Jiali Gao, David A. Bernlohr, Susan S. Taylor, Gianluigi Veglia*

*Corresponding author. Email: vegli001@umn.edu

Published 28 August 2019, *Sci. Adv.* **5**, eaaw9298 (2019)
DOI: 10.1126/sciadv.aaw9298

This PDF file includes:

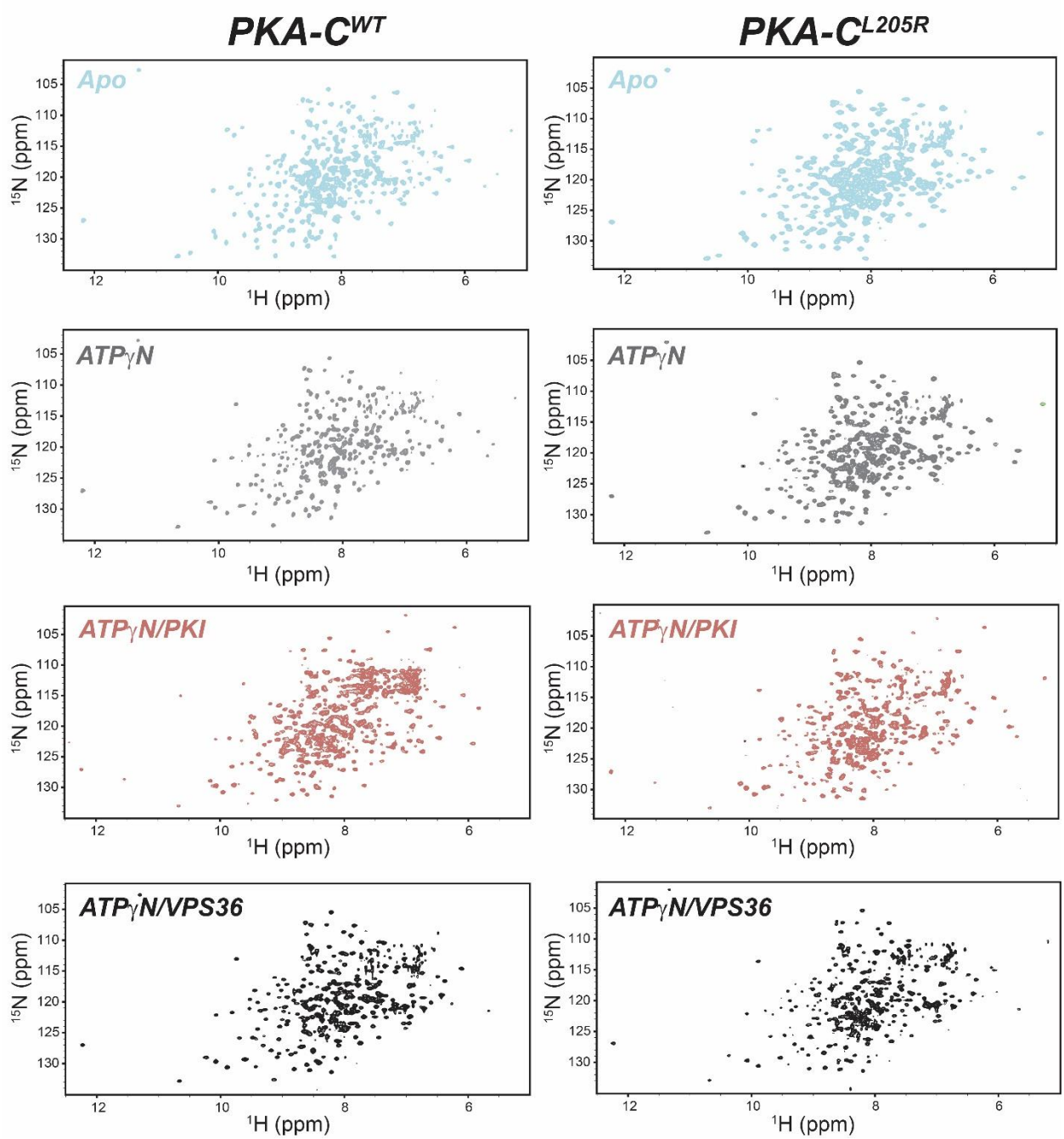

Fig. S1. [^{1}H, ^{15}N]-TROSY-HSQC spectra for PKA-C^{WT} and PKA-C^{L205R} in apo, ATPγN, and ATPγN/PKI-bound and ATPγN/VPS36-bound forms.

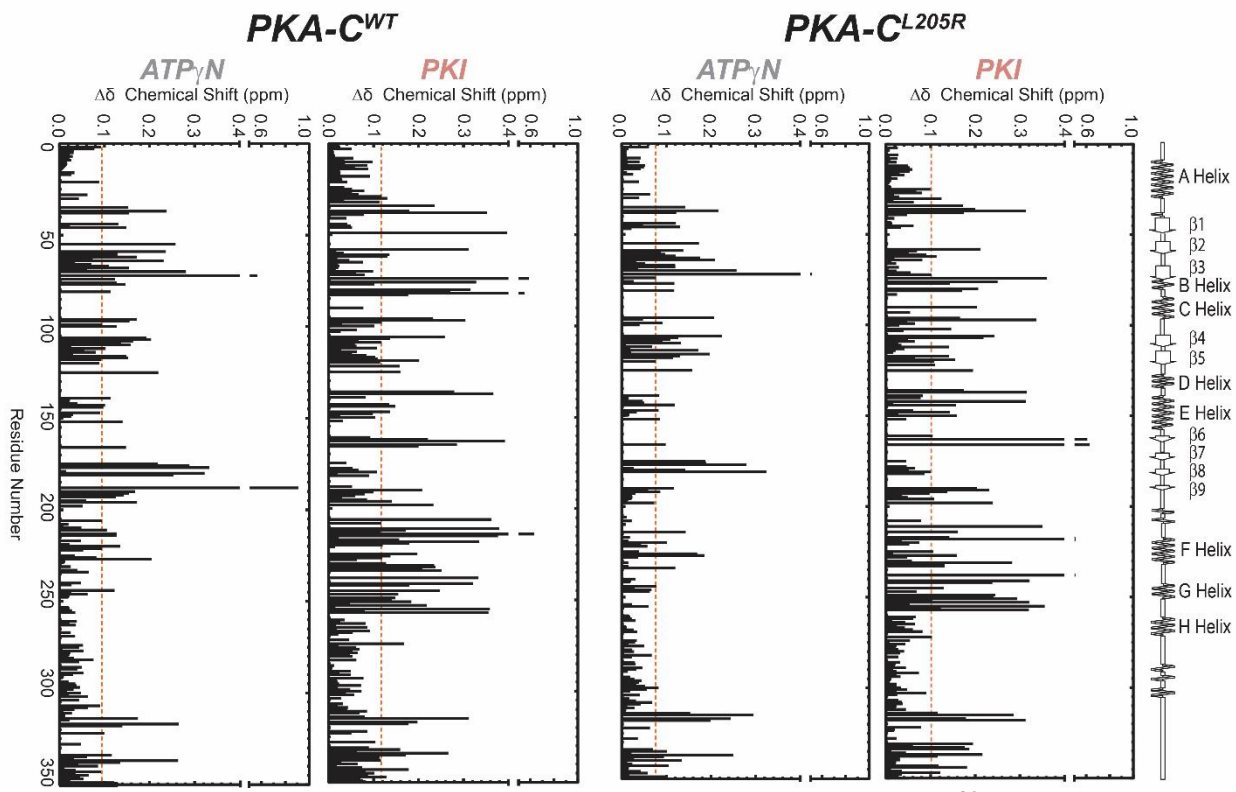

Fig. S2. CSPs observed upon ligand binding for PKA-C^{WT} and PKA-C^{L205R}. Histograms show the combined $^{1}H/^{15}N$ chemical shift perturbations vs. residue. The cutoff for the average Δδ are given as an orange dashed line.

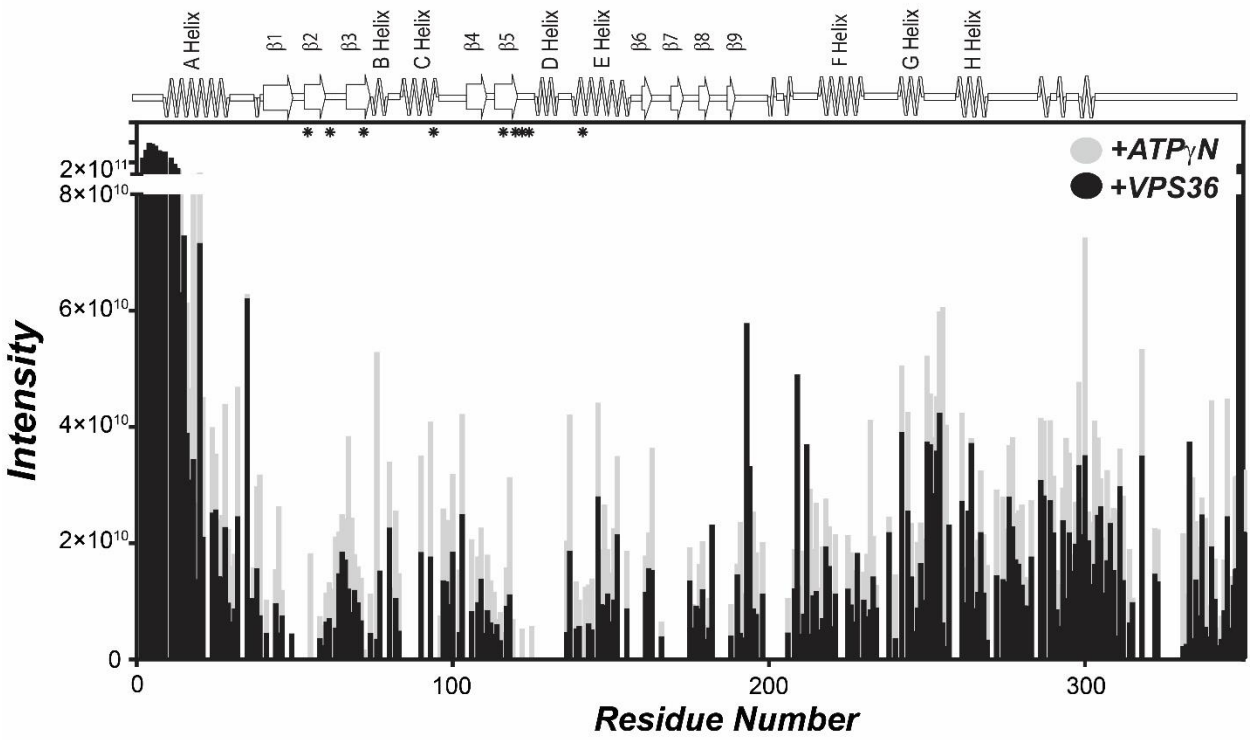

Fig. S3. Intensity plot for the binding of VPS36 to ATPγN-saturated PKA-C^{L205R}. Asterisks indicate residues that are broadened beyond detection. Intensity was corrected to account for the increase in number of scans following addition of VPS36 and was normalized to the noise level.

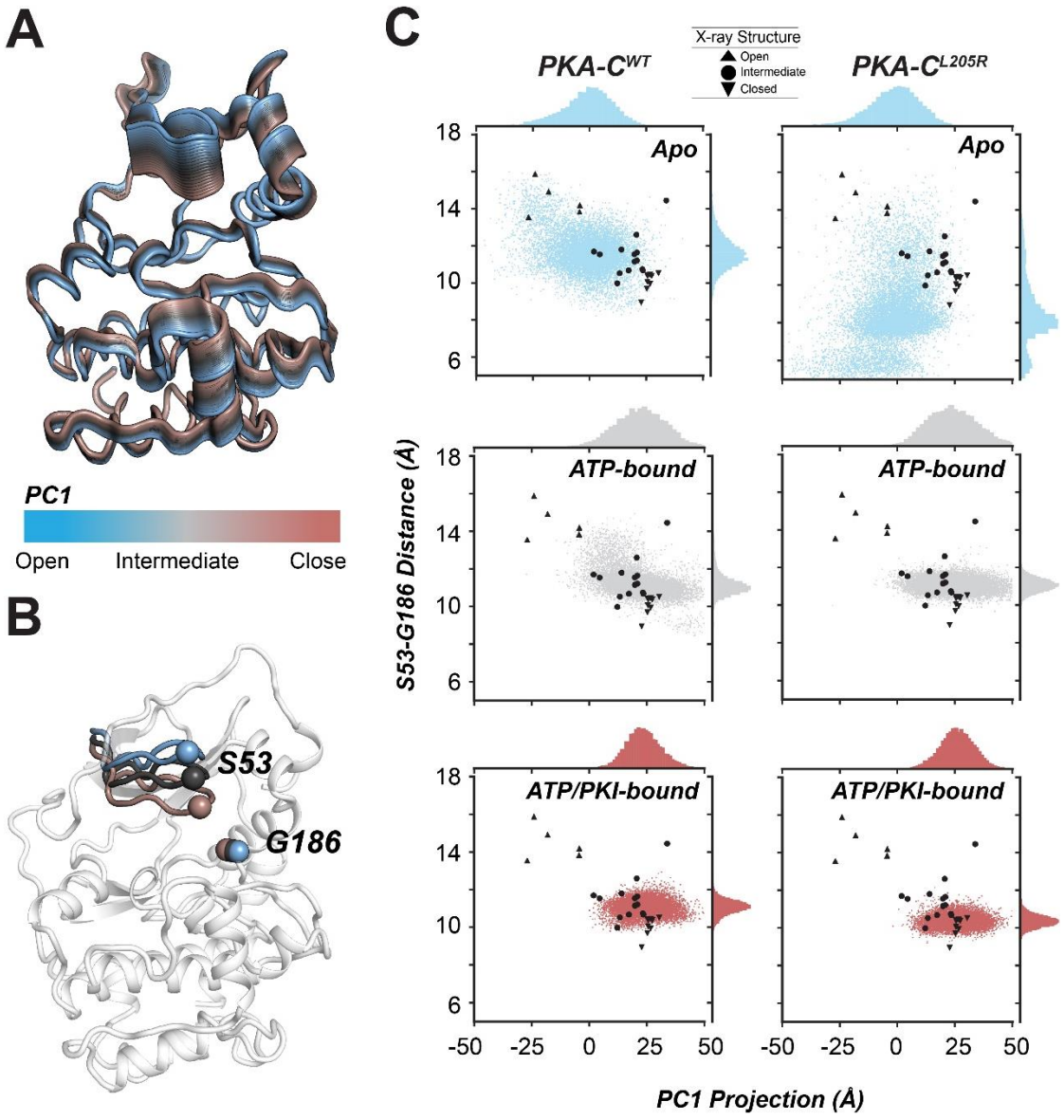

Fig. S4. PCA of the catalytic lobes in PKA-C^{WT} and PKA-C^{L205R}. (**A**) The first principal component of the catalytic lobes differentiates the open, intermediate and closed conformations. (**B**) The distances between Cα of S53 and G186 characterize the motion of Gly-rich loop. (**C**) 2D-scattering plot along dS53-G186 and PC1, and the corresponding distribution plots for PKA-C^{WT} (cyan), PKA-C^{WT} /ATP (gray) and PKA-C^{WT} /ATP/PKI (dark pink). Right panel: 2D-scattering plot along dS53-G186 and PC1, and the corresponding distribution plots for PKA-C^{L205R} (cyan), PKA-C^{L205R}/ATP (gray) and PKA-C^{L205R}/ATP/PKI (dark pink). The black shapes correspond to the projection of crystallographic conformations.

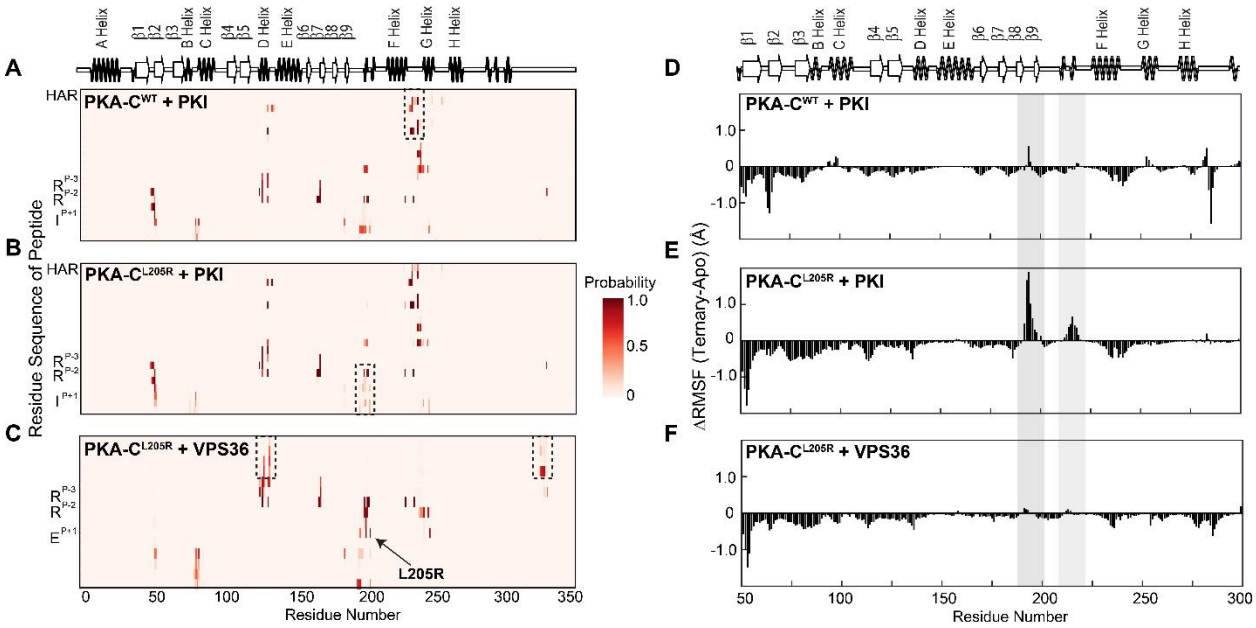

Fig. S5. Probability of the formation of inter-residue contact and ΔRMSF of PKA-C upon forming ternary complexes with PKI$_{5–24}$ or VPS36. The probability distribution of the distances for (**A**) PKA-C^{WT} and PKI highlighting stable contact between HAR of PKI and C-lobe of PKA-C^{WT}, (**B**) PKA-C^{L205R} and PKI highlighting the weakened interaction around the activation loop of PKA-C^{L205R}, and (**C**) PKA-C^{L205R} and VPS36 highlighting the stable contact at R205 and the transient contact of the N-terminal region of VPS36 with the hinge region and C-terminal tail of PKA-C^{L205R}. The probability distribution of the distances is defined by a cutoff of 5 Å between heavy atoms of residue pairs. The ΔRMSF of (**D**) PKA-C^{WT} against the apo state upon forming ternary complex with PKI, (**E**) PKA-C^{L205R} against apo state upon forming ternary complex with PKI, and (**F**) PKA-C^{L205R} against apo state upon forming ternary complex with VPS36.

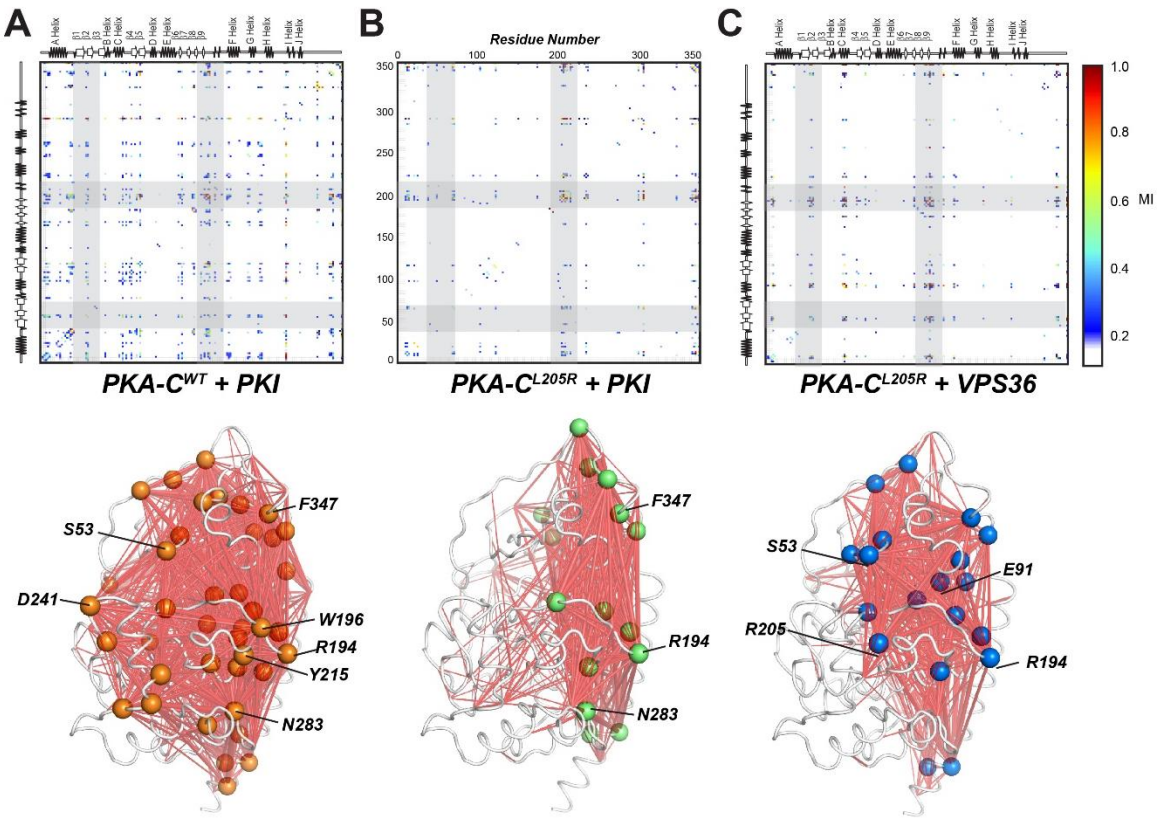

Fig. S6. Allosteric changes upon peptide binding revealed by MD simulation and mutual information (MutInf) analysis. Mufinf matrices of (**A**) PKA-C^{WT} in complex with PKI, (**B**) PKA-C^{L205R} in complex with PKI, and (**C**) PKA-C^{L205R} in complex with VPS36. Mutinf matrices are mapped to the structures of PKA-C^{WT} and PKA-C^{L205R} with a cutoff of 0.15.

Table S1. Changes in enthalpy, entropy, free energy, and dissociation constant of binding ATPγN, $PKI_{5–24}$, and VPS36 for PKA-C^{WT} and PKA-C^{L205R}. Errors in ΔG, ΔH, -TΔS, and K_d were calculated using triplicate measurements. Errors in σ were propagated from error in K_d. ND (not detected) indicates that the heat released upon binding is below the detection of the instrument. N/A indicates the value is not applicable to the particular measurements.

ATPγN to apo forms					
	K_d (μM)	**ΔG (kcal/mol)**	**ΔH (kcal/mol)**	**-TΔS (kcal/mol)**	**σ**
PKA-C^{WT}	83 ± 8	-5.61 ± 0.06	-3.6 ± 0.1	- 2.0 ± 0.1	N/A
PKA-C^{L205R}	215 ± 15	-5.04 ± 0.04	-6.2 ± 0.3	1.1 ± 0.2	N/A
PKI_{5-24} to apo forms					
	K_d (μM)	**ΔG (kcal/mol)**	**ΔH (kcal/mol)**	**-TΔS (kcal/mol)**	**σ**
PKA-C^{WT}	17 ± 2	-6.57 ± 0.08	-10.8 ± 0.5	4.2 ± 0.5	N/A
PKA-C^{L205R}	61 ± 5	-5.79 ± 0.04	-9.7 ± 0.1	3.9 ± 0.1	N/A
PKI_{5-24} to ATPγN saturated forms					
	K_d (μM)	**ΔG (kcal/mol)**	**ΔH (kcal/mol)**	**-TΔS (kcal/mol)**	**σ**
PKA-C^{WT}	0.16 ± 0.02	-9.33 ± 0.07	-13.9 ± 0.5	4.6 ± 0.4	106 ± 18
PKA-C^{L205R}	10 ± 3	-6.9 ± 0.2	-8.8 ± 0.8	1.9 ± 0.6	6 ± 2
VPS36 to ATPγN saturated forms					
	K_d (μM)	**ΔG (kcal/mol)**	**ΔH (kcal/mol)**	**-TΔS (kcal/mol)**	**σ**
PKA-C^{WT}	ND	ND	ND	ND	N/A
PKA-C^{L205R}	3.5 ± 0.1	-7.51 ± 0.03	-3.2 ± 0.6	-4.3 ± 0.6	N/A

Table S2. Kinetic parameters of Kemptide and VPS36 phosphorylation by PKA-C^{WT} and PKA-C^{L205R}. Values for K_M and k_{cat} were obtained from a non-linear least squares analysis of the concentration-dependent initial phosphorylation rates using a standard coupled enzyme activity assay (related to fig. S4). Error in k_{cat}/K_M was propagated from error in K_M and k_{cat}.

Kemptide		
	PKA-C^{WT}	**PKA-C^{L205R}**
V_{max} (μM/sec)	0.42 ± 0.02	0.90 ± 0.02
K_M (μM)	29 ± 1	335 ± 17
k_{cat} (s^{-1})	19 ± 1	41 ± 1
k_{cat}/K_M	0.66 ± 0.04	0.12 ± 0.01
VPS36		
	PKA-C^{WT}	**PKA-C^{L205R}**
V_{max} (μM/sec)	0.12 ± 0.02	0.39 ± 0.01
K_M (μM)	224 ± 48	326 ± 20
k_{cat} (s^{-1})	5 ± 1	18 ± 1
k_{cat}/K_M	0.022 ± 0.006	0.055 ± 0.004

Table S3. PCA and SD of the CONCISE analysis of the structural states analyzed.

	PCA1	SD	% Closed
PKA-C^{WT} *Apo*	-1.213	0.56	0%
PKA-C^{L205R} *Apo*	-1.042	0.57	7%
PKA-C^{WT} *ATPγN*	-0.059	0.56	45%
PKA-C^{L205R} *ATPγN*	-0.082	0.53	44%
PKA-C^{WT} *ATPγN/PKI*	1.335	0.61	100%
PKA-C^{L205R} *ATPγN/PKI*	0.904	0.55	83%
PKA-C^{WT} *ATPγN/VPS36*	-0.072	0.54	45%
PKA-C^{L205R} *ATPγN/VPS36*	0.229	0.79	57%

Table S4. T_m as determined using CD. All values are in °C and T_m was taken as the inflection point at which 50% of the enzyme complex was folded. Error was calculated using triplicate measurements.

	Apo	**Binary (MgATP)**	**Ternary (MgATP + PKI_{5-24})**
PKA^{WT}	53.2 ± 0.5	55.0 ± 0.7	60.2 ± 0.4
PKA^{L205R}	53.2 ± 0.4	56.7 ± 0.2	58.0 ± 0.3